



---

## Restoration algorithms for imaging through atmospheric turbulence

Jerome Gilles  
SAN DIEGO STATE UNIVERSITY FOUNDATION

---

03/06/2017  
Final Report

DISTRIBUTION A: Distribution approved for public release.

Air Force Research Laboratory  
AF Office Of Scientific Research (AFOSR)/ RTB1  
Arlington, Virginia 22203  
Air Force Materiel Command

REPORT DOCUMENTATION PAGE					Form Approved OMB No. 0704-0188	
The public reporting burden for this collection of information is estimated to average 1 hour per response, including the time for reviewing instructions, searching existing data sources, gathering and maintaining the data needed, and completing and reviewing the collection of information. Send comments regarding this burden estimate or any other aspect of this collection of information, including suggestions for reducing the burden, to the Department of Defense, Executive Services and Communications Directorate (0704-0188). Respondents should be aware that notwithstanding any other provision of law, no person shall be subject to any penalty for failing to comply with a collection of information if it does not display a currently valid OMB control number.						
PLEASE DO NOT RETURN YOUR FORM TO THE ABOVE ORGANIZATION.						
1. REPORT DATE (DD-MM-YYYY) 02-18-2017		2. REPORT TYPE Final Performance Report			3. DATES COVERED (From - To) Feb 2015 - Jan 2017	
4. TITLE AND SUBTITLE Restoration algorithms for imaging through atmospheric turbulence				5a. CONTRACT NUMBER		
				5b. GRANT NUMBER FA9550-15-1-0065		
				5c. PROGRAM ELEMENT NUMBER		
6. AUTHOR(S) Dr. Jerome Gilles				5d. PROJECT NUMBER		
				5e. TASK NUMBER		
				5f. WORK UNIT NUMBER		
7. PERFORMING ORGANIZATION NAME(S) AND ADDRESS(ES) Department of Mathematics & Statistics, San Diego State Univeristy 5500 Campanile Dr, San Diego, CA 92182					8. PERFORMING ORGANIZATION REPORT NUMBER	
9. SPONSORING/MONITORING AGENCY NAME(S) AND ADDRESS(ES) Air Force Office of Scientific Research (AFOSR), 875 N. Randolph Road, Arlington, VA 22203					10. SPONSOR/MONITOR'S ACRONYM(S)  AFOSR	
					11. SPONSOR/MONITOR'S REPORT NUMBER(S)	
12. DISTRIBUTION/AVAILABILITY STATEMENT DISTRIBUTION A						
13. SUPPLEMENTARY NOTES						
14. ABSTRACT This research project had focused on algorithms for imaging through atmospheric turbulence. An open data-set, called OTIS (Open Turbulent Image Set), was created for the community for algorithms assessment. A new wavelet burst accumulation method was proposed to reconstruct a restored image from a sequence of frames. We proposed a new spatio-temporal point of view for the moving object detection problem and we designed a vector field decomposition algorithm to numerically solved this problem. Finally, we mention some work currently in progress about a lucky imaging based super-resolution algorithm, as well as our current work on the simplification of the Fried kernel for deconvolution purposes.						
15. SUBJECT TERMS						
16. SECURITY CLASSIFICATION OF:			17. LIMITATION OF ABSTRACT	18. NUMBER OF PAGES	19a. NAME OF RESPONSIBLE PERSON	
a. REPORT	b. ABSTRACT	c. THIS PAGE			19b. TELEPHONE NUMBER (Include area code)	
U	U	U	U	22		

## INSTRUCTIONS FOR COMPLETING SF 298

**1. REPORT DATE.** Full publication date, including day, month, if available. Must cite at least the year and be Year 2000 compliant, e.g. 30-06-1998; xx-06-1998; xx-xx-1998.

**2. REPORT TYPE.** State the type of report, such as final, technical, interim, memorandum, master's thesis, progress, quarterly, research, special, group study, etc.

**3. DATES COVERED.** Indicate the time during which the work was performed and the report was written, e.g., Jun 1997 - Jun 1998; 1-10 Jun 1996; May - Nov 1998; Nov 1998.

**4. TITLE.** Enter title and subtitle with volume number and part number, if applicable. On classified documents, enter the title classification in parentheses.

**5a. CONTRACT NUMBER.** Enter all contract numbers as they appear in the report, e.g. F33615-86-C-5169.

**5b. GRANT NUMBER.** Enter all grant numbers as they appear in the report, e.g. AFOSR-82-1234.

**5c. PROGRAM ELEMENT NUMBER.** Enter all program element numbers as they appear in the report, e.g. 61101A.

**5d. PROJECT NUMBER.** Enter all project numbers as they appear in the report, e.g. 1F665702D1257; ILIR.

**5e. TASK NUMBER.** Enter all task numbers as they appear in the report, e.g. 05; RF0330201; T4112.

**5f. WORK UNIT NUMBER.** Enter all work unit numbers as they appear in the report, e.g. 001; AFAPL30480105.

**6. AUTHOR(S).** Enter name(s) of person(s) responsible for writing the report, performing the research, or credited with the content of the report. The form of entry is the last name, first name, middle initial, and additional qualifiers separated by commas, e.g. Smith, Richard, J, Jr.

**7. PERFORMING ORGANIZATION NAME(S) AND ADDRESS(ES).** Self-explanatory.

**8. PERFORMING ORGANIZATION REPORT NUMBER.** Enter all unique alphanumeric report numbers assigned by the performing organization, e.g. BRL-1234; AFWL-TR-85-4017-Vol-21-PT-2.

**9. SPONSORING/MONITORING AGENCY NAME(S) AND ADDRESS(ES).** Enter the name and address of the organization(s) financially responsible for and monitoring the work.

**10. SPONSOR/MONITOR'S ACRONYM(S).** Enter, if available, e.g. BRL, ARDEC, NADC.

**11. SPONSOR/MONITOR'S REPORT NUMBER(S).** Enter report number as assigned by the sponsoring/monitoring agency, if available, e.g. BRL-TR-829; -215.

**12. DISTRIBUTION/AVAILABILITY STATEMENT.** Use agency-mandated availability statements to indicate the public availability or distribution limitations of the report. If additional limitations/ restrictions or special markings are indicated, follow agency authorization procedures, e.g. RD/FRD, PROPIN, ITAR, etc. Include copyright information.

**13. SUPPLEMENTARY NOTES.** Enter information not included elsewhere such as: prepared in cooperation with; translation of; report supersedes; old edition number, etc.

**14. ABSTRACT.** A brief (approximately 200 words) factual summary of the most significant information.

**15. SUBJECT TERMS.** Key words or phrases identifying major concepts in the report.

**16. SECURITY CLASSIFICATION.** Enter security classification in accordance with security classification regulations, e.g. U, C, S, etc. If this form contains classified information, stamp classification level on the top and bottom of this page.

**17. LIMITATION OF ABSTRACT.** This block must be completed to assign a distribution limitation to the abstract. Enter UU (Unclassified Unlimited) or SAR (Same as Report). An entry in this block is necessary if the abstract is to be limited.

## **AFOSR Final Performance Report**

**Project title:** Restoration algorithms for imaging through atmospheric turbulence

**Award Number:** FA9550-15-1-0065

**Start Date:** Feb. 1st, 2015

**End Date:** Jan. 31st, 2017

**Project Manager:** Dr. Arje Nachman  
Program Officer, Electromagnetics  
875 North Randolph Road  
Ste 325, Room 3112  
Arlington, VA 22203  
Phone: 703-696-8427  
FAX: 703-696-8450  
Email: arje.nachman@us.af.mil

**Principal Investigator:** Prof. Jérôme Gilles  
Department of Mathematics & Statistics  
San Diego State University  
5500 Campanile Dr  
San Diego, CA, 92182-7720  
Phone: 619-594-7240  
FAX: 619-594-6746  
Email: jgilles@mail.sdsu.edu

# 1 Introduction

In the past decades several different long-range imaging systems were developed working in both the visible and infrared spectral bands. A direct consequence of imaging distant scenes is the effects of the atmosphere. Especially the presence of turbulence, which become non-negligible and affect the final resolution, limiting the efficiency of identifying a possible target. Several image processing algorithms were proposed to reduce the impact of the atmosphere and to reconstruct an image with better resolution and without geometrical deformations, see [1, 15, 16, 19, 23, 21, 22, 24, 25, 28, 30, 32, 36, 42, 44, 45] just to cite a few. The purpose of this project was to explore new restoration approaches; to improve some existing techniques (like the Fried deconvolution [19]), and investigate how moving target detection and tracking can be done within the framework of atmospheric turbulence.

## 2 Accomplishments

During this two years project, we realized three main tasks:

- We created a open dataset of static and dynamic sequences of observations through atmospheric turbulence in order for the community to create fair assessments of developed algorithms. An undergraduate student was involved in this project. This work was published in J. Gilles, N.B. Ferrante, "Open Turbulent Image Set (OTIS)", Pattern Recognition Letters, Vol.86, 38–41, 2017, DOI: 10.1016/j.patrec.2016.12.020.
- Based on the recent idea of Fourier Burst Accumulation deblurring, we proposed several combinations of Wavelet Burst Accumulation deblurring. We also adapted these techniques to take into account the non-rigid deformations due to the turbulence. This work was published in J. Gilles, S. Osher, "Wavelet burst accumulation for turbulence mitigation", Journal of Electronic Imaging, Vol.25, No.3, 033003-1–033003-9, May 2016. DOI: 10.1117/1.JEI.25.3.033003.
- We proposed a new approach to detect moving objects through atmospheric turbulence. The key idea is to consider geometric and oscillating patterns in the space+time space. This work involved a group of undergraduate and graduate students during the Summer 2016 within the context of a REU (Research Experience for Undergraduate) project funded by the NSF (my colleague Prof. V.Ponomarenko is the program director in our department); and was submitted to SIAM Imaging Sciences Journal.

The following sections give a description of about these different contributions.

## 3 Open Turbulence Image Set (OTIS)

Most turbulence mitigation papers in the literature use data which are not freely available hence making fair comparisons difficult. It becomes necessary to build an open dataset of images as well as to select some metric which can be used by the community in order to get an objective comparison of the different developed algorithms. In this section, we describe such an open dataset we created in San Diego thanks to funds from a university grant which allowed us to buy the basic equipments. This dataset is made of a collection of sequences of static scenes as well as dynamic scenes (i.e with a moving target). Most of the static sequences correspond to the observation of printed charts. Such approach permits to create a groundtruth associated to each sequence and then can be used by some metric to assess the reconstruction efficiency. We categorized the observed turbulence as either “weak”, “medium” or “strong”.

The work described in this section was published in J. Gilles, N.B. Ferrante, "Open Turbulent Image Set (OTIS)", Pattern Recognition Letters, Vol.86, 38–41, 2017, DOI: 10.1016/j.patrec.2016.12.020.

### 3.1 Equipment and acquisition procedure

#### 3.1.1 Equipment

All sequences were acquired with a GoPro Hero 4 Black camera modified with a RibCage Air chassis permitting to adapt several type of lenses. We always used a 25mm, f/2.0 14d HFOV 3MP lens. The camera was setup at a 1080p resolution and a framerate of 24 frames per second (fps). The camera was controlled by the standard GoPro App on a Samsung Galaxy tablet.

The acquired sequences contain both natural elements from the observed scene as well as artificial “targets”. For the static sequences, we used two charts containing some geometric patterns at different spatial frequencies and orientations (see left two images of Figure 1). These charts were printed on a poster (each chart has a size of 35x35cm) and held up by a homemade wooden stand. For the dynamic sequences, we used a standard remote controlled car (see right image of Figure 1).

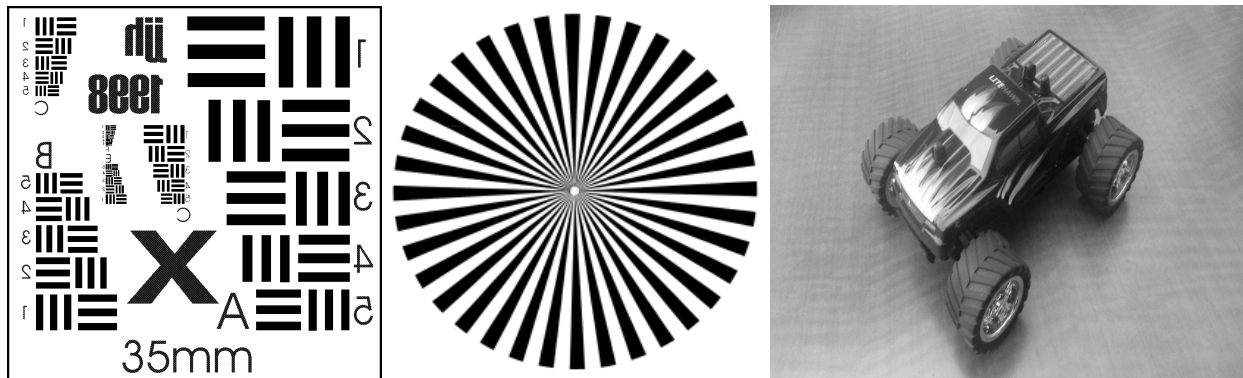


Figure 1: Two left images: the two charts serving as our static artificial targets after being printed on a poster. Right image: remote Controlled car utilized as our moving target for the dynamic sequences

#### 3.1.2 Procedures

All acquisitions were made on hot sunny days in order to guaranty a certain amount of atmospheric turbulence. All equipments were setup on a practice field at the San Diego State University. This field is equipped with artificial turf which reflects very well the sun heat, leading to high level of turbulence. The camera stood at about 10cm above the ground observing the target positioned at several distances.

After all acquisitions were done, the different recorded movies were downloaded on a Linux computer and split into sequences of PNG image files using the *ffmpeg* command<sup>1</sup>. The different region of interest were finally cropped via the *convert* command (from the *imagemagick* library<sup>2</sup>) and saved as individual PNG sequences. Since the Matlab® software is widely used by the community, we also provide each sequence as a Matlab 3D matrix, saved in a .mat file.

Since the purpose of this dataset is to be used for evaluating turbulence mitigation algorithms, all sequences containing the two above mentioned charts are provided with a groundtruth image. This groundtruth image contains the pristine chart after being downsampled and registered to the actual sequence. In practice, we manually registered the pristine chart on a temporal average of the input sequence using the GIMP<sup>3</sup> software (this procedure is summarized in Figure 2). The dynamic sequences are also provided with their respective

<sup>1</sup><https://ffmpeg.org/>

<sup>2</sup><http://www.imagemagick.org/>

<sup>3</sup><https://www.gimp.org/>

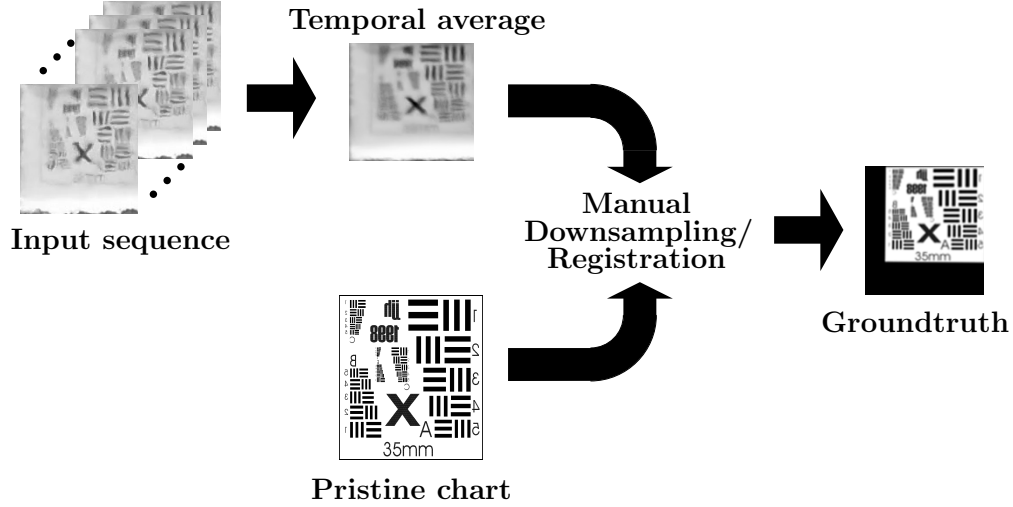


Figure 2: Groundtruth images creation procedure.

groundtruths. Each groundtruth is a sequence of binary images containing the bounding box corresponding to the moving target position. These groundtruths were created with the software *Sensarea*<sup>4</sup>.

### 3.2 Collected data

The different available sequences were acquired between June 18th and August 16th, 2016. We propose OTIS both in color and greyscale, it can be downloaded for free at <https://zenodo.org/communities/otis/>. Characteristics of static and dynamic sequences are given in Table 2 and 1, respectively. Samples frames are given in Figures 3 and 4.

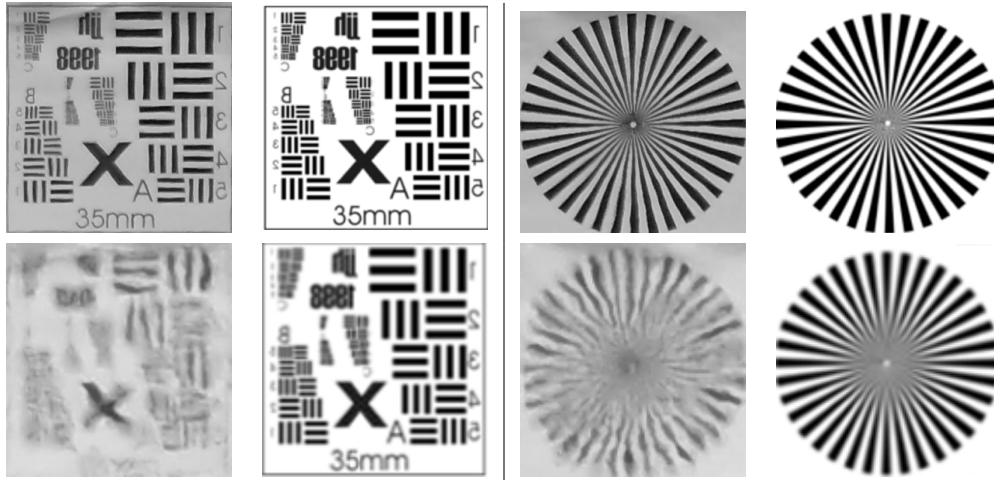


Figure 3: Samples of frames from different fixed pattern sequences and their corresponding groundtruths. The first row corresponds to a weak turbulence case while the second one corresponds to a strong turbulence case.

<sup>4</sup><http://www.gipsa-lab.grenoble-inp.fr/~pascal.bertolino/bin/download.php?file=sensarea.exe>

Table 1: Summary of the different dynamic sequences

Folder Name	Sequence Name	Number of images	Image size	Turbulence level	Ground Truth
Moving Target	Car1	100	200x200	Medium	Yes
	Car2	315	500x200	Medium	Yes
	Car3	51	300x300	Medium	Yes
	Car4	101	300x300	Medium	Yes

Table 2: Summary of the different static sequences

Folder Name	Sequence Name	Number of images	Image size	Turbulence level	Ground Truth
Fixed Background	Door	300	520x520	Strong	No
Fixed Patterns	Pattern1	64	302x309	Weak	Yes
	Pattern2	64	291x287	Weak	Yes
	Pattern3	300	113x117	Strong	Yes
	Pattern4	300	109x113	Strong	Yes
	Pattern5	300	113x117	Strong	Yes
	Pattern6	300	109x113	Strong	Yes
	Pattern7	300	122x125	Strong	Yes
	Pattern8	300	119x122	Strong	Yes
	Pattern9	300	152x157	Medium	Yes
	Pattern10	300	149x149	Medium	Yes
	Pattern11	300	172x183	Medium	Yes
	Pattern12	300	172x173	Medium	Yes
	Pattern13	300	202x202	Weak	Yes
	Pattern14	300	196x193	Weak	Yes
	Pattern15	300	134x139	Strong	Yes
	Pattern16	300	135x135	Strong	Yes

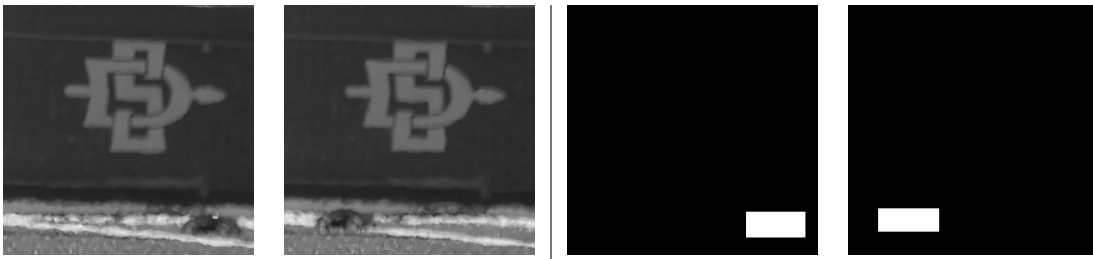


Figure 4: Frames 16 and 34 from a dynamic sequence and their corresponding groundtruth frames.

### 3.3 Quality metric

The main intent of OTIS is to facilitate the comparison of turbulence mitigation algorithms. Having test sequences as well as their groundtruth images is not sufficient to design a complete evaluation process. Indeed, it remains to choose some metrics in order to obtain an objective comparison. Denoting  $I_R$  and  $I_{GT}$  the restored and groundtruth images, respectively, the most used metric to compare images is the Mean Square Error (MSE) defined by

$$MSE(I_R, I_{GT}) = \frac{1}{N} \sum_x (I_R(x) - I_{GT}(x))^2,$$

where  $N$  is the number of pixel in the image. Despite its popularity, the MSE has several drawbacks, notably it doesn't take into account the geometric information contained within the image. The Structural Similarity Index Measure (SSIM) was proposed by [41] to circumvent these issues. The SSIM is a perception-based model which consider structural (geometrical) distortions in the image. Given the fact that one of the major degradation due to the turbulence is the geometrical distortions, the SSIM metric appears to be the most adapted metric to compare turbulence mitigation algorithms.

Regarding the assessment of tracking algorithms applied on the dynamic sequences, the methodology developed in [18] can be used.

## 4 Wavelet burst accumulation

In this section, we describe our investigation of the recently proposed weighted Fourier Burst Accumulation (FBA) method into the wavelet domain. The purpose of FBA is to reconstruct a clean and sharp image from a sequence of blurred frames. This concept lies in the construction of weights to amplify dominant frequencies in the Fourier spectrum of each frame. The reconstructed image is then obtained by taking the inverse Fourier transform of the average of all processed spectra. In this work, we first suggested to replace the rigid registration step used in the original algorithm by a non-rigid registration in order to be able to process sequences acquired through atmospheric turbulence. Second, we proposed to work in a wavelet domain instead of the Fourier one. This led us to the construction of two types of algorithms. Finally, we proposed an alternative approach to replace the weighting idea by an approach promoting the sparsity in the used space.

This work was published in: J. Gilles, S. Osher, "Wavelet burst accumulation for turbulence mitigation", Journal of Electronic Imaging, Vol.25, No.3, 033003-1–033003-9, May 2016. DOI: 10.1117/1.JEI.25.3.033003.

### 4.1 Fourier burst accumulation

We first recall the concept of weighted Fourier Burst Accumulation (FBA) proposed in [12] and we introduce some notations which will be used throughout this section. The aim of the FBA method is to retrieve a deblurred image of an original scene, denoted  $u$ , from a sequence of observations, assuming that those observations are affected by hand-shake blur. We will denote  $\{v_i\}_{i=1}^M$  the sequence of  $M$  observations such that,  $\forall i = 1, \dots, M$ ,

$$v_i(\mathbf{x}) = (k_i * u)(\mathbf{x}) + n_i(\mathbf{x}), \quad (1)$$

where  $*$  denotes the convolution product,  $\mathbf{x}$  the position in the image,  $n_i$  some noise and  $k_i$  is a blurring kernel affecting  $u$  at the frame  $i$ .

The authors of [12] defined the weighted Fourier Burst Accumulation (FBA) algorithm in the following

way: let  $p$  be a positive integer, the restored image,  $u_p$ , is obtained by

$$u_p(\mathbf{x}) = FBA(\{v_i(\mathbf{x})\}_{i=1}^M, p) = \mathcal{F}^{-1} \left( \sum_{i=1}^M w_i(\xi) \mathcal{F}(v_i)(\xi) \right) (\mathbf{x}), \quad (2)$$

$$\text{with } w_i(\xi) = \frac{G_\sigma(|\mathcal{F}(v_i)(\xi)|^p)}{\sum_{j=1}^M G_\sigma(|\mathcal{F}(v_j)(\xi)|^p)},$$

where  $\mathcal{F}$  denotes the Fourier transform ( $\xi$  are the frequencies) and  $G_\sigma$  is a Gaussian filter of standard deviation  $\sigma$ . The authors mention that the algorithm is not sensitive to the choice of  $\sigma$  and it can be automatically set to  $\sigma = \min(m_w, m_h)/50$  (where  $m_w$  and  $m_h$  are respectively the width and height of the image). In practice, the authors apply first a preprocessing registration step (they use a combination of SIFT [26] and ORSA [14] algorithms) in order to remove affine transformations (translations, rotations and homothety). The authors also suggest that optional denoising and sharpening final steps can be applied for contrast enhancement purposes.

This approach is based on the following principle: Fourier coefficients which represent an important information in the image must appear consistently in all observations. Therefore, the weights  $w_i(\xi)$  are large if Fourier coefficients  $\mathcal{F}(v_i)(\xi)$  are relatively stable through time, and weak otherwise. Then multiplying the Fourier spectrum of each observation by these weights will amplify the important information and attenuate time non-consistent information. Finally, an average spectrum is computed and  $u_p$  can be easily retrieved by inverse Fourier transform.

As mentioned above, the authors of [12] use an initial rigid registration step before applying the FBA algorithm. Unfortunately, for atmospheric turbulence mitigation purposes the observations are affected by non-rigid deformation and the use of a registration step based on SIFT and ORSA algorithms is inefficient. In [29], a non-rigid regularization technique was proposed to remove atmospheric non-rigid distortions. In particular, the deformation fields  $\Phi_i$  can be estimated via some optical-flow algorithm. We kept this non-rigid registration step. In details, it consists first to compute an average frame  $v_a(\mathbf{x}) = \frac{1}{M} \sum_{i=1}^M v_i(\mathbf{x})$ . Next, the deformation mappings  $\Phi_i$ , such that  $\forall i = 1, \dots, M; v_i = \Phi_i(v_a)$ , are estimated via an optical flow algorithm. Finally, the inverse mappings based on bilinear interpolations are applied to each frame:  $\Phi_i^{-1}(v_i) \rightarrow v_i$ . This registered sequence can then be used as the input of the burst accumulation methods.

## 4.2 Weighted wavelet burst accumulation

Other image representations than the Fourier representation are widely used in image processing, notably wavelet type representations (wavelets, framelets, curvelets, ...). Given a family of  $N$  wavelets  $\{\psi_n\}_{n=1}^N$ , the wavelet representation of an image  $v$  is given by the set of projections  $\{v^n\}_{n=1}^N = \{\langle v, \psi_n \rangle\}_{n=1}^N$ . In this paper, we will denote  $\mathcal{W}$  a wavelet type transform of the image  $v$ , i.e  $\{v^n\}_{n=1}^N = \mathcal{W}(v)$ . The inverse wavelet transform will be denoted  $\mathcal{W}^{-1}$ , i.e  $v = \mathcal{W}^{-1}(\{v^n\}_{n=1}^N)$ .

We can define two types of burst accumulation approaches. The first one processes the burst accumulation directly in the wavelet domain, we will denote it WWBA (Weighted Wavelet Burst Accumulation). Here, the weights are computed from the wavelet coefficients themselves, in each subband, amplifying the most dominant coefficients through time. The corresponding formulation is given by equations (3).

$$u_p(\mathbf{x}) = WWBA(\{v_i\}, \{\psi_n\}, p) = \mathcal{W}^{-1} \left( \left\{ \sum_{i=1}^M w_i^n(\mathbf{x}) v_i^n(\mathbf{x}) \right\}_{n=1}^N \right), \quad (3)$$

$$\text{with } w_i^n(\mathbf{x}) = \frac{G_\sigma(|v_i^n(\mathbf{x})|^p)}{\sum_{j=1}^M G_\sigma(|v_j^n(\mathbf{x})|^p)}.$$

The Gaussian filter,  $G_\sigma$ , is chosen as in the Fourier case.

The second type of accumulation consists in doing first the wavelet decomposition of each input frame. Then we apply the Fourier Burst Accumulation algorithm from [12] (recalled in Section 4.1) to each subband sequences  $\{v_i^n\}_{i=1}^M$ . We call this approach the Weighted Wavelet Fourier Burst Accumulation (WWFBA) and can be formulated by equations (4).

$$u_p(\mathbf{x}) = WWFBA(\{v_i\}, \{\psi_n\}, p) = \mathcal{W}^{-1} \left( \left\{ FBA(\{v_i^n(\mathbf{x})\}_{i=1}^M, p) \right\}_{n=1}^N \right). \quad (4)$$

This option is equivalent to deblur the wavelet coefficients themselves.

### 4.3 Mathematical characterization

In [12], the authors characterized the FBA algorithm with the following proposition.

**Proposition 1** *Applying the FBA algorithm on a sequence  $\{v_i\}_{i=1}^M$  provides a restored image  $u_p$  equivalent to*

$$u_p = k_e * u + \bar{n} \quad \text{where} \quad k_e = \mathcal{F}^{-1} \left( \sum_{i=1}^M w_i \mathcal{F}(k_i) \right), \quad (5)$$

and  $\bar{n}$  is the weighted average of the input noise.

We investigated the same kind of characterization for the two previously introduced algorithms in the wavelet domain. First, we need to switch to the filter bank point of view about the wavelet decomposition. In the previous section, we denoted the wavelet decomposition of  $v$  by  $\{v^n\}_{n=1}^N = \{\langle v, \psi_n \rangle\}_{n=1}^N$ . It is also well-known in wavelet theory, using the frame formalism [10], that it can be written as a convolution product:

$$\{v^n\}_{n=1}^N = \{v * \bar{\psi}_n\}_{n=1}^N, \quad (6)$$

where  $\bar{\psi}_n(\mathbf{x}) = \psi_n(-\mathbf{x})$ . The inverse wavelet transform is given by

$$v(\mathbf{x}) = \mathcal{W}^{-1}(\{v^n\}_{n=1}^N)(\mathbf{x}) = \sum_{n=1}^N (v^n * \psi_n)(\mathbf{x}). \quad (7)$$

Therefore, in the same formalism, the wavelet transform of each observed frame  $v_i$  can be written as (we omit  $\mathbf{x}$  in the following in order to simplify the notations)

$$\{v_i^n\}_{n=1}^N = \{v_i * \bar{\psi}_n\}_{n=1}^N = \{(k_i * u + n_i) * \bar{\psi}_n\}_{n=1}^N = \{k_i * u * \bar{\psi}_n\}_{n=1}^N + \{n_i * \bar{\psi}_n\}_{n=1}^N. \quad (8)$$

We thus obtain the following characterizations.

#### Analysis of the WWBA algorithm

The WWBA restoration algorithm proposed in the previous section is equivalent to

$$u_p = \sum_{i=1}^M \sum_{n=1}^N (w_i^n (k_i * u * \bar{\psi}_n)) * \psi_n + \sum_{i=1}^M \sum_{n=1}^N (w_i^n (n_i * \bar{\psi}_n)) * \psi_n. \quad (9)$$

Unfortunately, pointwise multiplication and convolution do not commute so it is not possible to write this expression as the convolution of  $u$  with some equivalent kernel as the authors did in [12] for the Fourier burst case.

## Analysis of the WWFBA algorithm

In the WWFBA algorithm case, we have the following proposition.

**Proposition 2** *Applying independent Fourier burst accumulations on each subband ( $n$ ) sequences  $\{v_i^n\}_{i=1}^M$  is equivalent to*

$$u_p = (k_e * u) + \bar{n} \quad \text{where} \quad k_e = \sum_{n=1}^N \sum_{i=1}^M \mathcal{F}^{-1}(w_i^n) * k_i * \bar{\psi}_n * \psi_n. \quad (10)$$

## 4.4 Non-linear burst accumulation

The frame accumulation techniques described in section 4.2 are all based on linear combination (either by pointwise multiplications or convolutions) of each frames in different representation domains. These weights basically correspond to amplify dominant coefficients thus we can ask if it is possible to exploit other approaches to perform such amplification? We proposed an alternative to the use of weights. Amplifying only the dominant coefficients can be interpreted in the sense that only those dominant coefficients are important to represent the image. Therefore, instead of using some amplification, we can imagine to keep the dominant coefficients and remove the other ones. In other words the restored image is expected to have a sparse representation in the used representation domains. It is then natural to promote the sparsity in each representation before doing the accumulation. In the last decade, the compressive sensing community widely developed such concepts. It is well established that minimizing models based on  $L^1$ -norm provide sparse solutions [20]. Let a function  $f$ , the simplest model to find a sparse representation  $g$  from  $f$  is given by (11),

$$g = \arg \min_{\tilde{g}} \|\tilde{g}\|_1 + \frac{1}{2\lambda} \|\tilde{g} - f\|_2^2. \quad (11)$$

It is well-known that the solution of this minimization problem is given by soft-thresholding  $f$  with threshold  $\lambda$ , and is given by (the operators are understood pointwise)

$$g = \text{Soft}(f, \lambda) = \frac{f}{|f|} \max(|f| - \lambda, 0). \quad (12)$$

Therefore, denoting  $\mathcal{D}$  the representation domain which can be either  $\mathcal{F}$  or  $\mathcal{W}$ , we propose the following general sparse burst accumulation model.

$$u_p(\mathbf{x}) = \text{SDBA}(\{v_i(\mathbf{x})\}_{i=1}^M, \lambda) = \mathcal{D}^{-1} \left( \sum_{i=1}^M \text{Soft}(\mathcal{D}(v_i), \lambda) \right) (\mathbf{x}). \quad (13)$$

Notice that in the case of a wavelet-type decomposition, the soft-thresholding operator is applied in each subband.

## 4.5 Experiments

In our experiments, we decided to use two popular families of wavelets in image processing: framelets and curvelets. Framelets are basically constructed in the same philosophy as for classic 2D tensor wavelets except that no downsampling is involved in the process. This particularity permits to guarantee translation invariant decompositions which is important for image processing. Moreover, it is well known that such family form a tight frame which ensures easy reconstructions and permits to have algorithms which are less sensitive to important loss of information (see [35] for more details). Curvelets also form a tight frame but

their main particularity is in the fact that they also capture directional information hence providing better representations of geometric structures in images (see [5, 8] for details).

In order to distinguish between the different algorithms, we will use the following acronyms:

- FBA: Fourier Burst Accumulation,
- Fr-WWBA: Framelet based Weighted Wavelet Burst Accumulation,
- C-WWBA: Curvelet based Weighted Wavelet Burst Accumulation,
- Fr-WWFBA: Framelet based Weighted Wavelet Fourier Burst Accumulation,
- C-WWFBA: Curvelet based Weighted Wavelet Fourier Burst Accumulation,
- SFBA: Sparse Fourier Burst Accumulation,
- Fr-SWBA: Framelet based Sparse Wavelet Burst Accumulation,
- C-SWBA: Curvelet based Sparse Wavelet Burst Accumulation.

We experiment the proposed algorithms on a sequence denoted Barchart 1 (frames 1 and 25 are illustrated in Figure 5). We ran all algorithms (FBA, Fr-WWBA, C-WWBA, Fr-WWFBA, C-WWFBA, SFBA, Fr-SWBA and C-SWBA) without any registration and with non-rigid registration. As suggested by the authors of [12], we fix  $p = 11$  for all weighted methods. For the sparse based methods, the parameter  $\lambda$  is set to  $\lambda = 0.5$  for SFBA and  $\lambda = 0.001$  for Fr-SWBA and C-SWBA. We used 50 frames in each test.

The Figure 6 presents the results obtained without any registration step. If, compared to the original frames, cleaner images are obtained, it is worth to notice that some geometric distortions remain in the reconstructed images thus comforting the idea that a non-rigid registration step is needed to deal with the turbulence problem.

The results obtained when using the non-rigid registration step are given in Figure 7. It is clear that the non-rigid registration step is essential to correct the geometric distortions induced by the turbulence. For instance, we can notice that vertical bars in the barchart are straighter and sharper than in either the original and restored without non-rigid registration images. Comparing the different methods with non-rigid registration, the wavelet based options give clearer restored images than the FBA technique. The advantage looks like to be in favor of the sparse options as they provide images with more contrast than the weighted approaches.

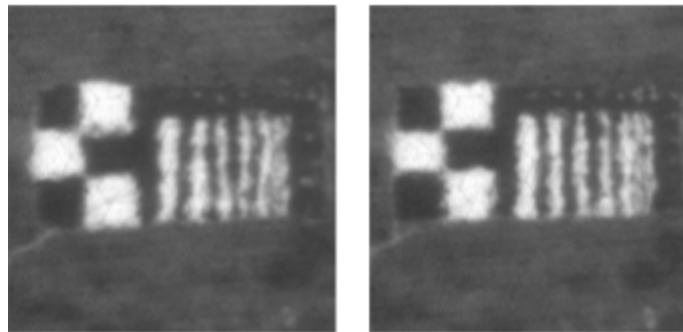


Figure 5: Original sequence Barchart 1. The consecutive columns correspond to the frames 1 and 25, respectively.

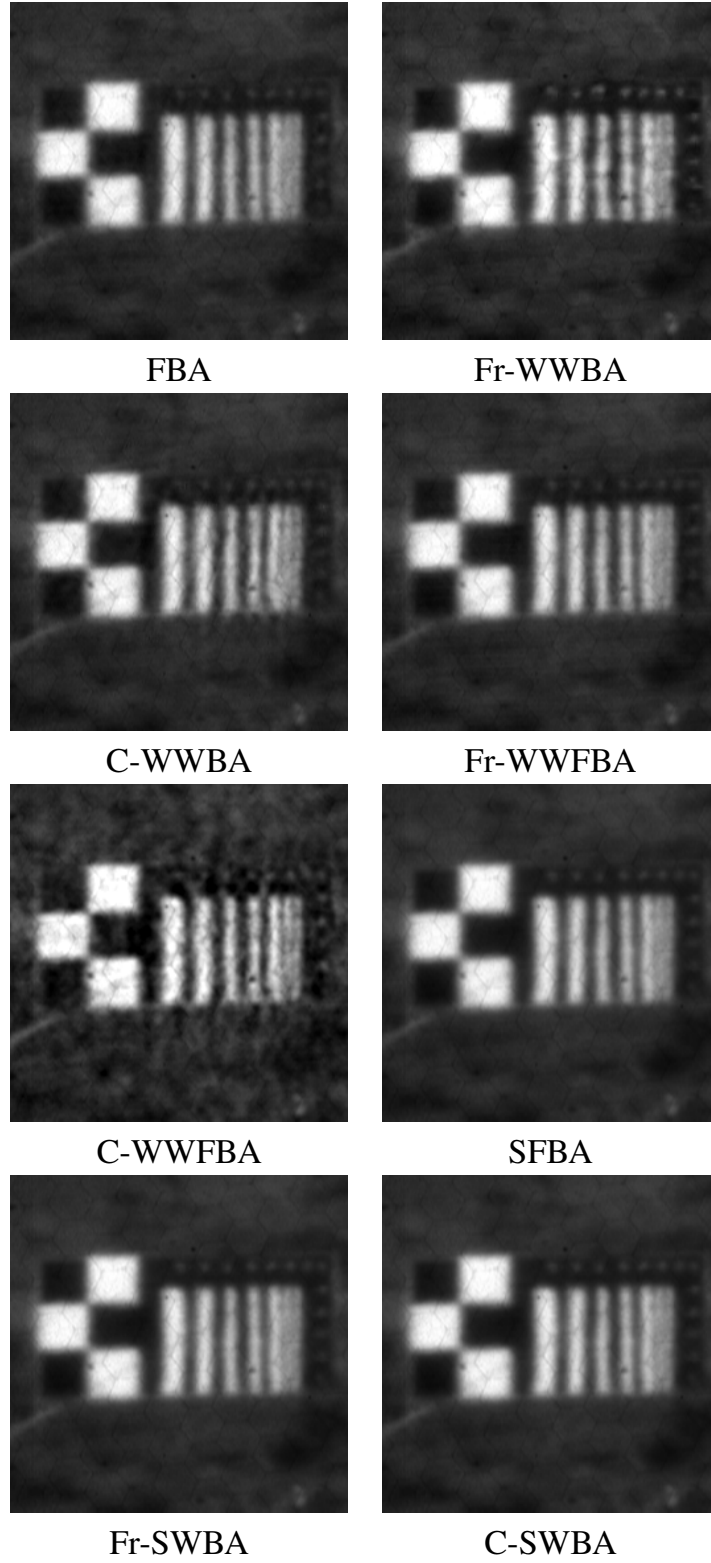


Figure 6: Restoration results on Barchart 1 sequence (50 frames) without non-rigid registration and  $p = 11$  (without any final denoising or sharpening step).

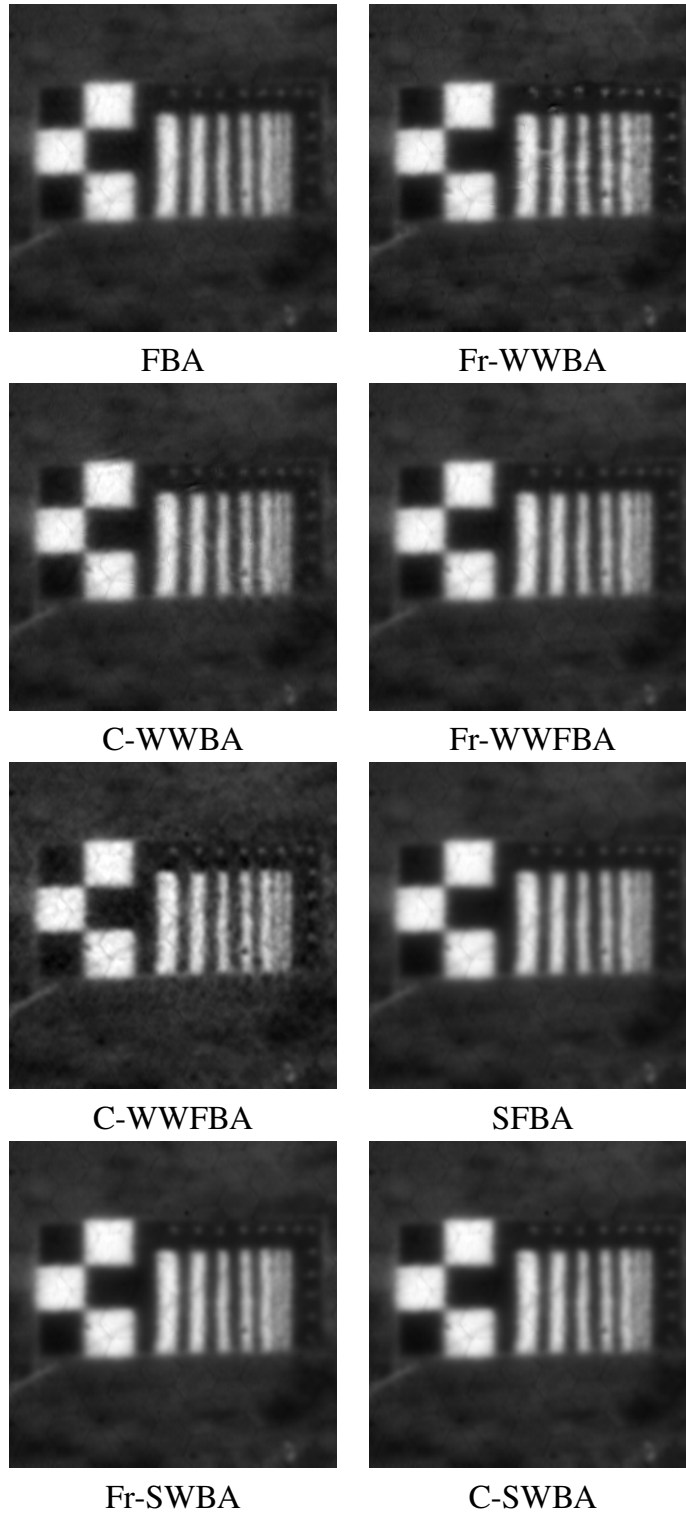


Figure 7: Restoration results on Barchart 1 sequence (50 frames) with non-rigid registration and  $p = 11$  (without any final denoising or sharpening step).

## 5 Moving target detection through turbulent media

In this section, we investigate how moving objects can be detected when images are impacted by atmospheric turbulence. We present a geometric spatio-temporal point of view of the problem and show that it is possible to distinguish movement due to the turbulence vs. moving objects. To perform this task, we propose to extend 2D cartoon+texture decomposition algorithms to 3D vector fields.

This work has been submitted to SIAM Imaging Science Journal: J. Gilles, F. Alvarez, N. Ferrante, M. Fortman, L. Tahir, A. Tarter, A. von Seeger, “Detection of moving objects through turbulent media. Decomposition of Oscillatory vs Non-Oscillatory spatio-temporal vector fields.”.

### 5.1 Moving objects in turbulent media

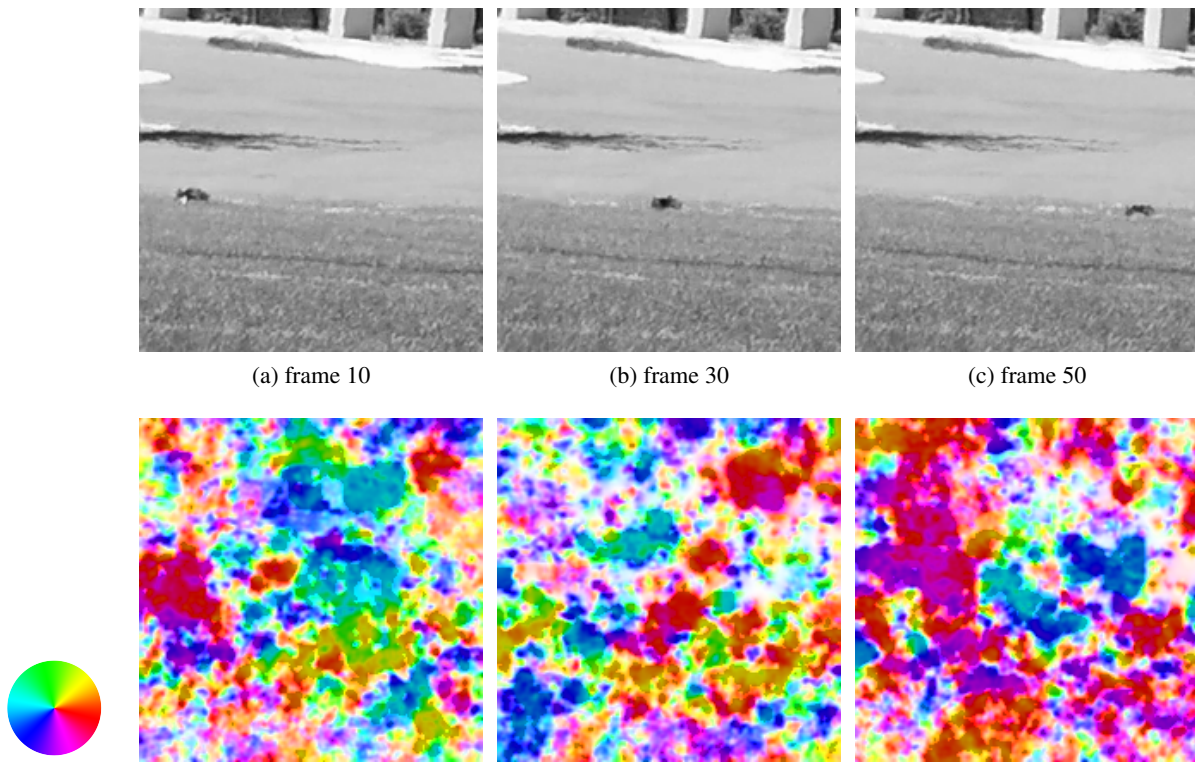


Figure 8: Several frames from the OTIS Car1 sequence. The second row shows the velocity vector field corresponding to each frame.

We start to illustrate the specificity of sequences impacted by the presence of atmospheric turbulence. Figures 8 and 9 present several frames from the sequences Car1 and Car2 from the Open Turbulent Image Set (OTIS) [17] described in Section 3. Clearly, the turbulence creates dynamic local deformations which are confirmed by the velocity vector fields given on the second row of each of those figures (the color wheel on the left gives the correspondence between the color and the vector direction). All pixels of all frames are clearly subject to some movement. Moreover, these vector fields are mainly made of random vectors (both in direction and magnitude). Therefore, it is almost impossible to distinguish the movement information which corresponds to moving object vs. moving atmosphere, therefore a new approach is needed. The standard vision of the problem is biased by the fact that we watch the sequence frame by frame (i.e. a temporal succession of 2D images). We suggested to consider the whole sequence as a single spatio-temporal space.

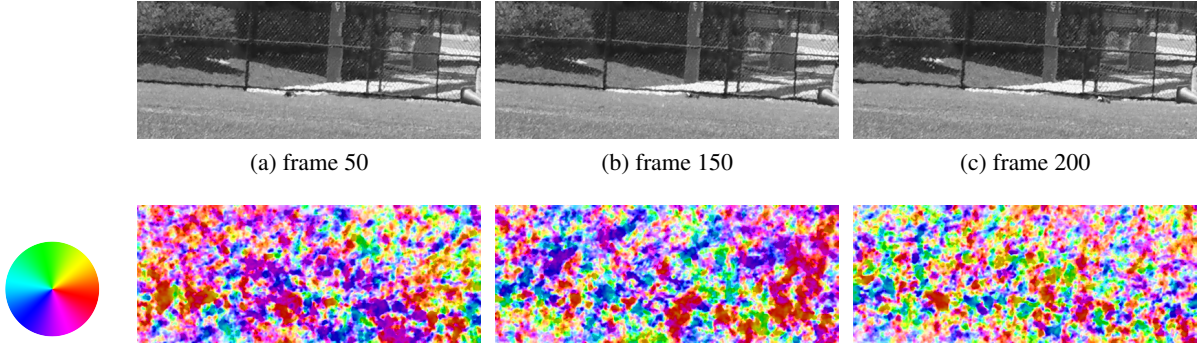


Figure 9: Several frames from the OTIS Car2 sequence. The second row shows the velocity vector field corresponding to each frame.

In particular, if we visualize the colored vector field as a 3D cube of data (i.e. each pixel in the 3D space is a vector), we can see the emergence of geometric patterns. Indeed, if the turbulence movement is random in both space and time, the movement of a moving object is expected to be “consistent”, i.e a moving object follows some trajectory which is not supposed to be erratic. This concept is illustrated in Figure 10 where slices corresponding to  $x - time$  planes ( $y$  is fixed) are given. This visualization confirms that a moving object creates a geometric pattern in the space-time volume while the atmospheric turbulence velocity field behaves like an oscillating function. Therefore, we suggest that detecting moving objects through atmospheric turbulence can be achieved by separating non-oscillating vs. oscillating components of the vector fields. This idea is explored in the next section.

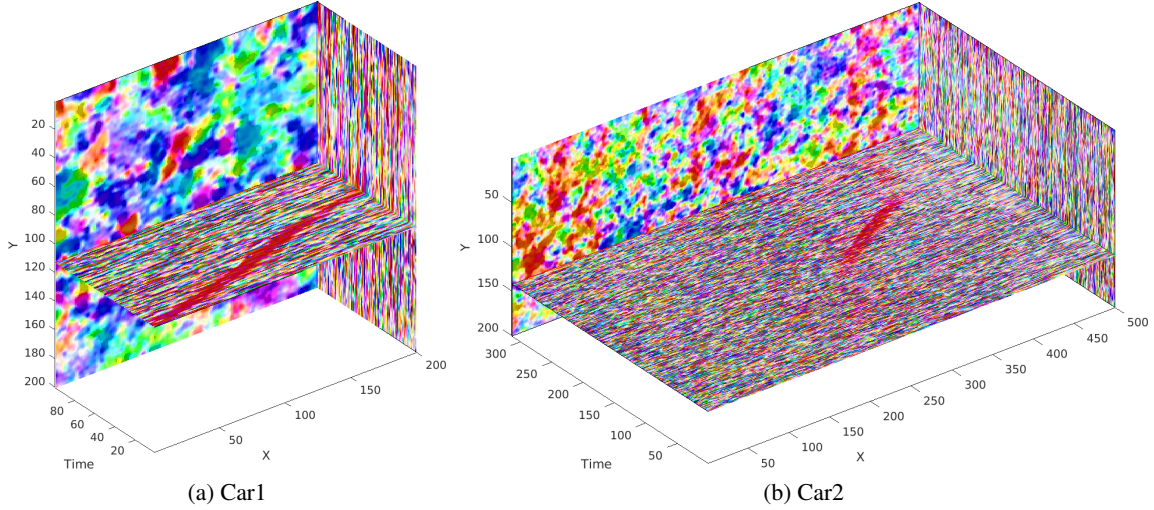


Figure 10: 3D spatio-temporal patterns visualization in the velocity vector fields of the Car1 and Car2 sequences.

## 5.2 Decomposition methods

The idea of separating oscillating vs. non-oscillating components has been widely studied in image processing. The specific purpose of these investigations was to separate the cartoon component from the texture component in a given image. The cartoon and texture parts correspond to non-oscillating and oscillating

function, respectively. In this work, we extended such type of algorithm to spatio-temporal vector fields. We first recall the formalism used in the image processing case and next we introduce the vector field case.

### 5.2.1 Image decomposition

Given an image  $f$ , the purpose of the cartoon + texture decomposition is to find two images  $u$  (the cartoon, i.e. piecewise constant function) and  $v$  (the textures, i.e. oscillating function) such that  $f = u + v$ . This concept was proposed by Meyer [31] in his investigation of the Rudin-Osher-Fatemi (ROF) model [34]. Several authors [2, 3, 4, 33, 38, 40] then proposed different modifications of Meyer’s model leading to tractable algorithms. In particular, the case of using Besov spaces [39],  $\dot{B}_{p,q}^s$  (we consider the homogeneous version of these spaces), is numerically interesting since Besov spaces can be characterized by the mean of wavelet coefficients [9, 11, 27]. Using the fact that  $\dot{B}_{1,1}^1 \subset BV$  and  $G \subset \dot{B}_{-1,\infty}^0$ , we can formulate a Besov based variational decomposition model by

$$(\hat{u}, \hat{v}) = \arg \min_{u \in \dot{B}_{1,1}^1, v \in \dot{B}_{-1,\infty}^0} \|u\|_{\dot{B}_{1,1}^1} + J_B^* \left( \frac{v}{\mu} \right) + (2\lambda)^{-1} \|f - (u + v)\|_{L^2}, \quad (14)$$

where

$$J_B^* \left( \frac{v}{\mu} \right) = \begin{cases} 0 & \text{if } \|v\|_{\dot{B}_{-1,\infty}^0} \leq \mu \\ +\infty & \text{otherwise} \end{cases}. \quad (15)$$

Such model can easily be solved by iterating soft thresholding of the wavelet coefficients. Denoting  $\mathcal{W}(f)$  the wavelet transform of  $f$  (we assume a real transform) and  $Shrink(x, \lambda) = \text{sign}(x) \max(0, x - \lambda)$ , the numerical algorithm can be resumed by Algorithm 1.

---

**Algorithm 1** Besov based decomposition numerical algorithm.

---

Inputs: image to decompose  $f$ , parameters  $\lambda, \mu$ , maximum number of iterations  $N_{max}$

Initialization:  $n = 0, u^0 = v^0 = 0$

**repeat**

$$v^{n+1} = f - u^n - \mathcal{W}^{-1} (Shrink(\mathcal{W}(f - u^n), 2\mu))$$

$$u^{n+1} = \mathcal{W}^{-1} (Shrink(\mathcal{W}(f - v^{n+1}), 2\lambda))$$

**until**  $\max(\|u^{n+1} - u^n\|_{L^2}, \|v^{n+1} - v^n\|_{L^2}) < 10^{-6}$  **or**  $N_{max}$  iterations are reached

**return**  $u^{n+1}, v^{n+1}$

---

### 5.2.2 Spatio-temporal vector field decomposition

Next, we extended the previous decomposition model to spatio-temporal vector fields. Let us denote  $f(i, j, n)$  the input sequence of  $N$  frames where  $i, j$  are the 2D spatial variables and  $n$  is the frame number. The decomposition model can be easily extended to 3D by simply using a 3D wavelet transform instead of the 2D one, while the algorithm itself remains unchanged. However, we want to decompose vector fields corresponding to the estimated velocity from frame to frame hence the previous algorithm must be adapted to vector fields. If we denote the spatio-temporal vector field  $\mathbf{v}(i, j, n) = (v_1(i, j, n), v_2(i, j, n))$ , the first idea which comes to mind is to process the vector field components  $v_1$  and  $v_2$  separately and then recompose the final vector field. Unfortunately, this approach will not perform well in some cases, like when one of the components is oscillating while the other is constant. We need to process the vector field as a single object. We can simply achieve this by rewriting the vector field as a complex vector field, i.e

$$\tilde{\mathbf{v}}(i, j, n) = v_1(i, j, n) + iv_2(i, j, n).$$

Now, we can use the same 3D decomposition algorithm only if we change the standard wavelet transform by a complex wavelet transform and then use the complex version of the thresholding operator defined by

$$\forall z = |z|e^{i\theta} \in \mathbb{C} \quad , \quad CShrink(z, \lambda) = \max(0, |z| - \lambda)e^{i\theta}.$$

Moreover, we suggest a last modification to the algorithm to better take into account geometric patterns with specific orientations. Indeed, as shown in the Figure 10, the pattern associated to the moving object correspond to a piecewise constant function with a direction not parallel to the space axis. Therefore, it is of interest to use a representation which takes into account such different orientations. The 3D classic wavelet transform is built on a tensor approach, i.e. is separable into three 1D transforms with respect to each axis, hence does not allow to take care of different orientations. An alternative to the classic wavelet transform is the curvelet transform [5, 6, 7, 8, 13, 37, 43] where the curvelet filters are built on angular wedges in the 3D Fourier space. Since, curvelets are wavelet type functions, it is possible to formalize curvelet based Besov spaces which we will denote  $\dot{C}_{p,q}^s$ . We can then replace the use of Besov spaces  $\dot{B}_{p,q}^s$  by curvelet spaces  $\dot{C}_{p,q}^q$  and the curvelet based decomposition model consists in solving model (16).

$$(\hat{u}, \hat{v}) = \arg \min_{u \in \dot{C}_{1,1}^1, v \in \dot{C}_{-1,\infty}^\infty} \|u\|_{\dot{C}_{1,1}^1} + J_C^* \left( \frac{v}{\mu} \right) + (2\lambda)^{-1} \|f - (u + v)\|_{L^2}, \quad (16)$$

where

$$J_C^* \left( \frac{v}{\mu} \right) = \begin{cases} 0 & \text{if } \|v\|_{\dot{C}_{-1,\infty}^\infty} \leq \mu \\ +\infty & \text{otherwise} \end{cases}. \quad (17)$$

If we denote  $\mathcal{C}$  the curvelet transform of  $f$ , the numerical algorithm which solves model (16) is given in Algorithm 2.

---

**Algorithm 2** Curvelet based decomposition numerical algorithm.

---

Inputs: image to decompose  $f$ , parameters  $\lambda, \mu$ , maximum number of iterations  $N_{max}$

Initialization:  $n = 0, u^0 = v^0 = 0$

**repeat**

$$v^{n+1} = f - u^n - \mathcal{C}^{-1} (CShrink(\mathcal{C}(f - u^n), 2\mu))$$

$$u^{n+1} = \mathcal{C}^{-1} (Shrink(\mathcal{C}(f - v^{n+1}), 2\lambda))$$

**until**  $\max(\|u^{n+1} - u^n\|_{L^2}, \|v^{n+1} - v^n\|_{L^2}) < 10^{-6}$  **or**  $N_{max}$  iterations are reached

**return**  $u^{n+1}, v^{n+1}$

---

### 5.3 Experimental results

In this section, we present the results obtained by Algorithm 2 on the sequences Car1 and Car2 from the OTIS dataset presented in Section 3. We experimentally observed that the choice  $\lambda = \mu = 1$  works well for all sequences and hence was used in all our experiments. The maximum number of iterations was fixed to  $N_{max} = 5$ . Figures 11 and 12 provide the geometric and oscillating components of the velocity vector fields corresponding to each sequence, respectively. As expected, the geometric component highlights the movement of the moving object while the oscillating component contains the turbulence movement. Even on the difficult sequence Car2 where the object is small, moves close to an edge from the background and hence is strongly affected by the turbulence, the algorithm does a good job. Furthermore, in order to have a comparison with Figure 10, we provide the spatio-temporal plots for the extracted components in Figure 13. Again, it is obvious to see that the expected geometric patterns corresponding to moving objects are enhanced in the geometric component making them easier to detect.

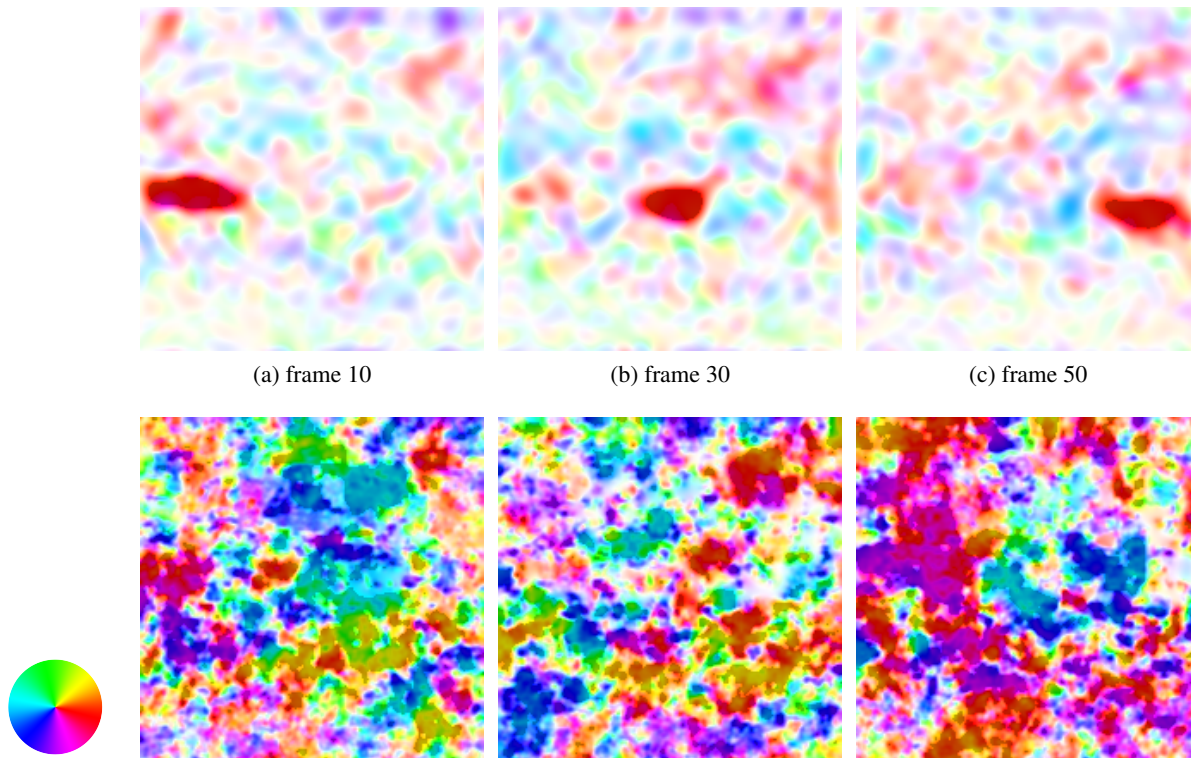


Figure 11: Decomposition results on the OTIS Car1 sequence. The first row corresponds to the geometric component and the second row the oscillating component.

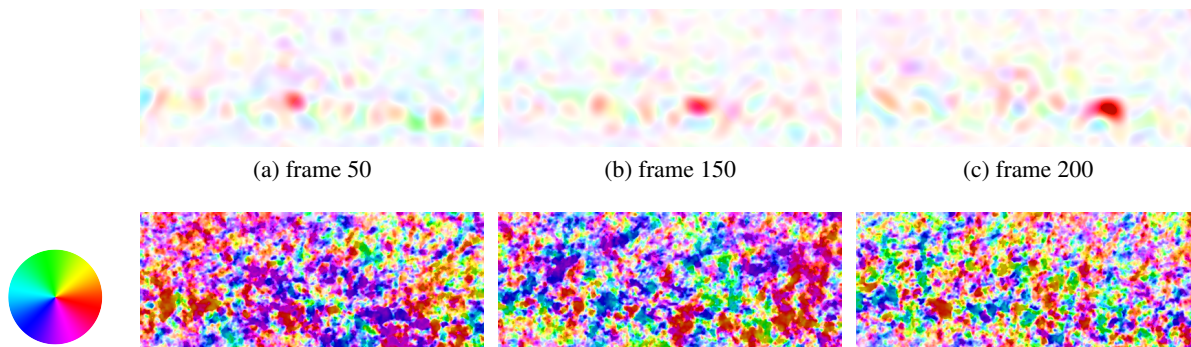


Figure 12: Decomposition results on the OTIS Car2 sequence. The first row corresponds to the geometric component and the second row the oscillating component.

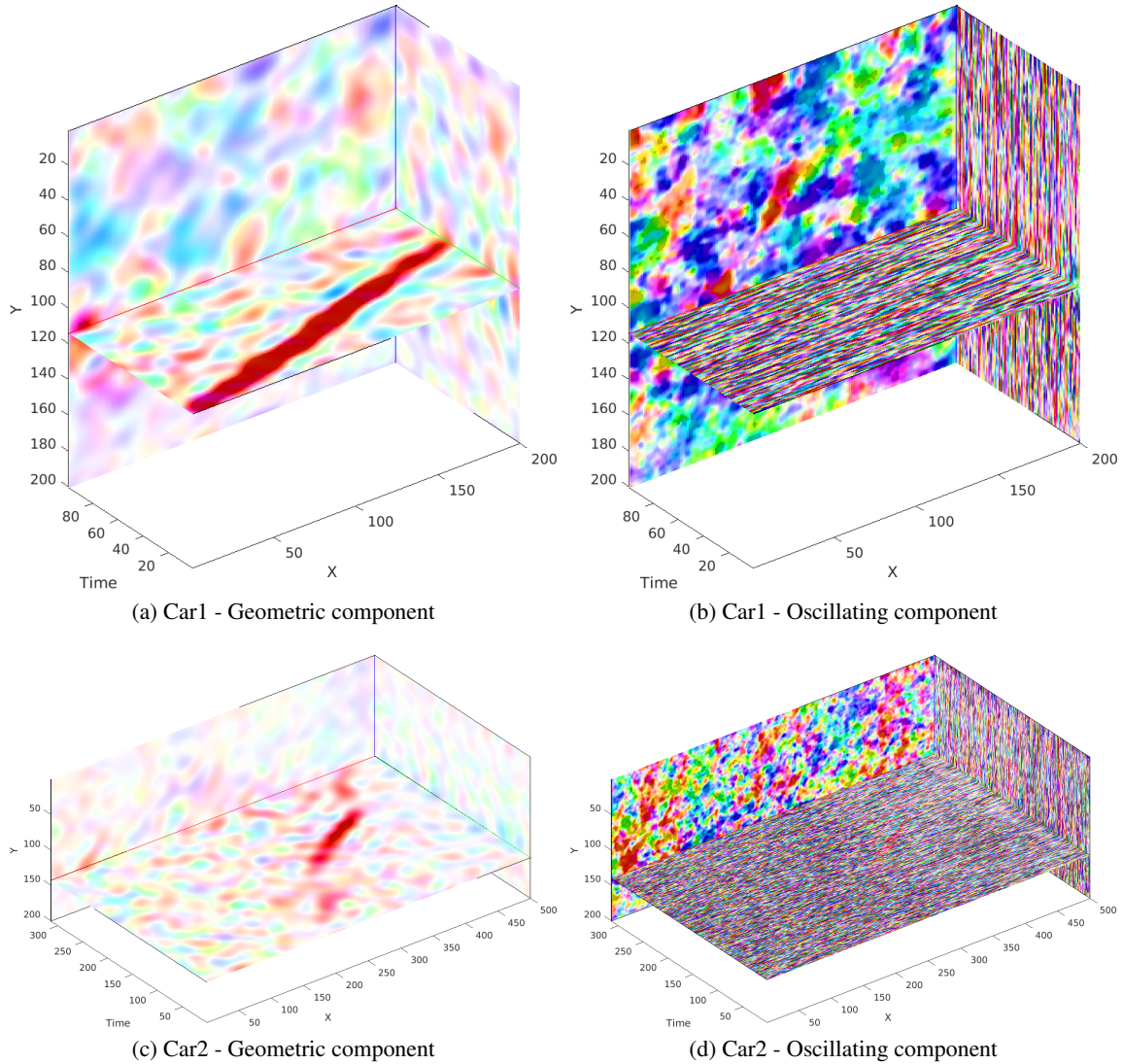


Figure 13: 3D spatio-temporal patterns visualization of the geometric and oscillating components of the Car1 and Car2 sequences velocity vector fields.

## 6 Work in progress

We are currently making progress on two topics: parameters estimation of the Fried deconvolution and the design of a lucky imaging super-resolution algorithm.

- The Fried kernel models the impact (in terms of blur) of the atmospheric turbulence in images and was used in [19] to perform the final deconvolution needed to get sharper images. The main issue with the current Fried formulation is the need to know four parameters. We started some investigation on mathematically simplifying the kernel with the goal of building an efficient method to estimate the remaining parameters. Unfortunately, our first experiments showed that the problem is much more complex than expected. In particular, priors used to characterize the parameters are non-convex. We recently started a collaboration with Dr. Charles Deledalle from France who just started a sabbatical year at UCSD. Dr. Deledalle is a specialist of parameter estimation. We are starting to investigate new approaches to solve this problem.

- The lucky imaging idea was proposed many years ago but in our opinion, it is completely under-exploited. A SDSU graduate student, Francis Alvarez, is currently working on this topic for his master's thesis. Our idea is that the atmosphere locally behaves like an optical lens. The presence of turbulence locally modify this behavior in the sense that the atmosphere can correspond to either a zoom in or zoom out effect. A good idea is then to keep only the information corresponding to a zoom in, while getting rid of the information from zoom out regions. Doing so, we can expect to keep only the best information from the sequence to reconstruct a restored image and we even expect to be able to do some very efficient super-resolution. As of today, we already found how to distinguish zoom in vs. zoom out regions in a given frame. We are currently working on how this information can be incorporated in a super-resolution algorithm.

## References

- [1] Nantheera Anantrasirichai, Alin Achim, Nick G. Kingsbury, and David R. Bull. Atmospheric turbulence mitigation using complex wavelet-based fusion. *IEEE Transaction in Image Processing*, 22(6):2398–2408, June 2013.
- [2] Jean-François Aujol, Gilles Aubert, Laure Blanc-Féraud, and Antonin Chambolle. *Image Decomposition Application to SAR Images*, pages 297–312. Springer Berlin Heidelberg, 2003.
- [3] J.F. Aujol and A. Chambolle. Dual norms and image decomposition models. *International Journal of Computer Vision*, 63(1):85–104, 2005.
- [4] J.F. Aujol, G. Gilboa, T. Chan, and S. Osher. Structure-texture image decomposition-modeling, algorithms and parameter selection. *International Journal of Computer Vision*, 67(1):111–136, 2006.
- [5] E. Candès, L. Demanet, D. Donoho, and L. Ying. Fast discrete curvelet transforms. *Multiscale Modeling and Simulation*, 5(3):861–899, 2005.
- [6] E. Candès and D. Donoho. Continuous curvelet transform, part I: Resolution of the wavefront set. *Applied and Computational Harmonic Analysis*, 19(2):162–197, 2005.
- [7] E. Candès and D. Donoho. Continuous curvelet transform, part II: Discretization and frames. *Applied and Computational Harmonic Analysis*, 19(2):198–222, 2005.
- [8] Emmanuel Candès and David Donoho. Curvelets: A surprisingly effective nonadaptive representation of objects with edges. In L. L. Schumaker et al., editor, *Curves and Surfaces*. Vanderbilt University Press, 1999.
- [9] A. Chambolle, R.A. DeVore, N. Lee, and B.J. Lucier. Nonlinear wavelet image processing: variational problems, compression and noise removal through wavelet shrinkage. *IEEE Trans. on Image Processing*, 7(3):319–335, 1998.
- [10] Ole Christensen. Frames, riesz bases, and discrete gabor/wavelet expansions. *Bulletin of the American Mathematical Society*, 38(3):273–291, 2001. [doi:10.1090/S0273-0979-01-00903-X].
- [11] I. Daubechies. *Ten lectures on wavelets*. Society for Industrial and Applied Mathematics, 1992.
- [12] Mauricio Delbracio and Guillermo Sapiro. Removing camera shake via weighted fourier burst accumulation. *IEEE Transaction in Image Processing*, 24(11):3293–3307, November 2015. [doi:10.1109/TIP.2015.2442914].

- [13] D. Donoho and M. Duncan. Digital curvelet transform: strategy, implementation and experiments. volume 4056 of *Proceedings SPIE, Wavelet Applications VII*, 2000.
- [14] M. Fisher and R. Bolles. Random sample consensus: A paradigm for model fitting with applications to image analysis and automated cartography. *Communications of the ACM*, 24(6):381–395, 1981. [doi:10.1145/358669.358692].
- [15] D. H. Frakes, J. W. Monaco, and M. J. T. Smith. Suppression of atmospheric turbulence in video using an adaptive control grid interpolation approach. *IEEE Conference Proceedings on Acoustics, Speech and Signal Processing*, 3:1881–1884, 2001.
- [16] S. Gepshtein, A. Shtainman, and B. Fishbain. Restoration of atmospheric turbulent video containing real motion using rank filtering and elastic image registration. In *Proceedings of EUSIPCO*, Vienna, Austria, September 2004.
- [17] J. Gilles and N.B. Ferrante. Open Turbulent Image Set (OTIS). *Pattern Recognition Letters*, 86:38–41, 2017.
- [18] Jérôme Gilles, Stéphane Landeau, Tristan Dagobert, Philippe Chevalier, Eric Stié, Damien Diaz, and Jean-Luc Maillart. METRIC: a complete methodology for performances evaluation of automatic target detection, recognition and tracking algorithms in infrared imagery. In *OPTRO 2010*, Paris, France, February 2010.
- [19] Jérôme Gilles and Stanley Osher. Fried deconvolution. In *SPIE Defense, Security and Sensing conference*, Baltimore, US, April 2012.
- [20] Tom Goldstein and Stanley Osher. The split Bregman method for  $L^1$  regularized problems. *SIAM Journal on Imaging Sciences*, 2(2):323–343, 2009. [doi:10.1137/080725891].
- [21] Kalyan Kumar Halder, Murat Tahtali, and Sreenatha G. Anavatti. High precision restoration method for non-uniformly warped images. In *Advanced Concepts for Intelligent Vision Systems - 15th International Conference, ACIVS, Proceedings*, volume 8192 of *Lecture Notes in Computer Science*, pages 60–67, Poznan, Poland, October 28-31 2013. Springer.
- [22] Kalyan Kumar Halder, Murat Tahtali, and Sreenatha G. Anavatti. Model-free prediction of atmospheric warp based on artificial neural network. *Applied Optics*, 53(30):7087–7094, October 2014.
- [23] K.K. Halder, M. Tahtali, and S.G. Anavatti. A fast restoration method for atmospheric turbulence degraded images using non-rigid image registration. In *2013 International Conference on Advances in Computing, Communications and Informatics (ICACCI)*, pages 394–399, Mysore, 2013.
- [24] Dalong Li, Russell M. Mersereau, and Steven Simske. Atmospheric turbulence-degraded image restoration using principal components analysis. *IEEE Geoscience and Remote Sensing Letters*, 4(3):340–344, July 2007.
- [25] Yifei Lou, Sung Ha Kang, Stefano Soatto, and Andrea L. Bertozzi. Video stabilization of atmospheric turbulence distortion. *Inverse Problems and Imaging*, 7(3):839–861, 2013.
- [26] David G. Lowe. Object recognition from local scale-invariant features. In *Proceedings of the International Conference on Computer Vision*, volume 2, pages 1150–1157, 1999. [doi:10.1109/ICCV.1999.790410].
- [27] S. Mallat. *A wavelet tour of signal processing*. Academic Press, 1999.

- [28] Yu Mao and Jérôme Gilles. Non rigid geometric distortions correction - application to atmospheric turbulence stabilization. *Journal of Inverse Problems and Imaging*, 6(3):531–546, 2012.
- [29] Yu Mao and Jérôme Gilles. Non rigid geometric distortions correction - application to atmospheric turbulence stabilization. *Journal of Inverse Problems and Imaging*, 6(3):531–546, 2012.
- [30] Enric Meinhardt-Llopis and Mario Micheli. Implementation of the Centroid Method for the Correction of Turbulence. *Image Processing On Line*, 4:187–195, 2014.
- [31] Y. Meyer. *Oscillating patterns in image processing and in some nonlinear evolution equations*. The Fifteenth Dean Jacqueline B. Lewis Memorial Lectures, American Mathematical Society, 2001.
- [32] M. Micheli, Y. Lou, S. Soatto, and A. Bertozzi. A linear systems approach to imaging through turbulence. *Journal of Mathematical Imaging and Vision*, 48(1):185–201, 2014.
- [33] S. Osher, A. Sole, and L. Vese. Image decomposition and restoration using total variation minimization and the  $H^{-1}$  norm. *Multiscale Modeling and Simulation: A SIAM Interdisciplinary Journal*, 1(3):349–370, 2002.
- [34] L. Rudin, S. Osher, and E. Fatemi. Nonlinear total variation based noise removal algorithms. *Physica D*, 60(1–4):259–268, 1992.
- [35] I.W. Selesnick and A. Farras Abdelnour. Symmetric wavelet tight frames with two generators. *Applied and Computational Harmonic Analysis*, 17(2):211–225, September 2004. [doi:10.1016/j.acha.2004.05.003].
- [36] Changxin Song, Ke Ma, Anqiang Li, Xiaofang Chen, and Xing Xu. Diffraction-limited image reconstruction with SURE for atmospheric turbulence removal. *Infrared Physics & Technology*, 71:171–174, 2015.
- [37] J.L. Starck, E. Candès, and D. Donoho. The curvelet transform for image denoising. *IEEE Trans. Image Processing*, 11(6):670–684, 2002.
- [38] J.L. Starck, M. Elad, and D.L. Donoho. Image decomposition: separation of texture from piecewise smooth content. volume 5207. SPIE conference on Signal and Image Processing: Wavelet Applications in Signal and Image Processing X, SPIE’s 48th Annual Meeting, San Diego, 2003.
- [39] H. Triebel. *Theory of function spaces II*. Birkhäuser Basel, 1992.
- [40] L. Vese and S. Osher. Modeling textures with total variation minimization and oscillating patterns in image processing. *Journal of Scientific Computing*, 19(1-3):553–572, 2003.
- [41] Z. Wang, A.C. Bovik, H.R. Sheikh, and E.P. Simoncelli. Image quality assessment: from error visibility to structural similarity. *IEEE Trans on Image Processing*, 13(4):600–612, April 2004.
- [42] Bo Yang, Wensheng Zhang, Yuan Xie, and Qingchun Li. Distorted image restoration via non-rigid registration and lucky-region fusion approach. In *Proceedings of the Third International Conference on Information Science and Technology*, pages 414–418, Yangzhou, Jiangsu, China, March 23-25 2013.
- [43] Lexing Ying, Laurent Demanet, and Emmanuel Candès. 3D discrete curvelet transform. In *Optics & Photonics 2005*, pages 591413–591413. International Society for Optics and Photonics, 2005.

- [44] Xiang Zhu and Peyman Milanfar. Image reconstruction from videos distorted by atmospheric turbulence. In *SPIE Electronic Imaging, Conference 7543 on Visual Information Processing and Communication*, San Jose, CA, USA, 2010.
- [45] Christine M. Zwart, Richard J. Pracht, and David H. Frakes. Improved motion estimation for restoring turbulence distorted video. In *Proceedings of SPIE*, volume 8355 of *Infrared Imaging Systems: Design, Analysis, Modeling, and Testing XXIII*, pages 83550E–1–83550E–9, 2012.

# AFOSR Deliverables Submission Survey

Response ID:7674 Data

1.

---

**Report Type**

Final Report

---

**Primary Contact Email**

Contact email if there is a problem with the report.

jgilles@mail.sdsu.edu

---

**Primary Contact Phone Number**

Contact phone number if there is a problem with the report

6195947240

---

**Organization / Institution name**

San Diego State University

---

**Grant/Contract Title**

The full title of the funded effort.

Restoration algorithms for imaging through atmospheric turbulence

---

**Grant/Contract Number**

AFOSR assigned control number. It must begin with "FA9550" or "F49620" or "FA2386".

FA9550-15-1-0065

---

**Principal Investigator Name**

The full name of the principal investigator on the grant or contract.

Dr. Jerome Gilles

---

**Program Officer**

The AFOSR Program Officer currently assigned to the award

Dr. Arje Nachman

---

**Reporting Period Start Date**

02/01/2015

---

**Reporting Period End Date**

01/31/2017

---

**Abstract**

In the past decades several different long-range imaging systems were developed working in both the visible and infrared spectral bands. A direct consequence of imaging distant scenes is the effects of the atmosphere. Especially the presence of turbulence, which become non-negligible and affect the final resolution, limiting the efficiency of identifying a possible target. In this project, we investigated image processing techniques within the framework of atmospheric turbulence. We proposed a new restoration approach based on a wavelet burst accumulation method. We proposed a new approach to perform moving target detection affect by turbulence. We also built an open dataset of sequences with either fixed background or with a moving target, available for the community to fairly assess developed algorithms.

---

**Distribution Statement**

DISTRIBUTION A: Distribution approved for public release.

This is block 12 on the SF298 form.

Distribution A - Approved for Public Release

### Explanation for Distribution Statement

If this is not approved for public release, please provide a short explanation. E.g., contains proprietary information.

### SF298 Form

Please attach your [SF298](#) form. A blank SF298 can be found [here](#). Please do not password protect or secure the PDF. The maximum file size for an SF298 is 50MB.

[SF298-Filled.pdf](#)

Upload the Report Document. File must be a PDF. Please do not password protect or secure the PDF. The maximum file size for the Report Document is 50MB.

[Final\\_Report2017.pdf](#)

Upload a Report Document, if any. The maximum file size for the Report Document is 50MB.

### Archival Publications (published) during reporting period:

J. Gilles, N.B. Ferrante, "Open Turbulent Image Set (OTIS)", Pattern Recognition Letters, Vol.86, 38–41, 2017, DOI: 10.1016/j.patrec.2016.12.020.

J. Gilles, S. Osher, "Wavelet burst accumulation for turbulence mitigation", Journal of Electronic Imaging, Vol.25, No.3, 033003-1–033003-9, May 2016. DOI: 10.1117/1.JEI.25.3.033003.

J. Gilles, F. Alvarez, N. Ferrante, M. Fortman, L. Tahir, A. Tarter, A. von Seeger, "Detection of moving objects through turbulent media. Decomposition of Oscillatory vs Non-Oscillatory spatio-temporal vector fields", Submitted to SIAM Imaging Journal.

### New discoveries, inventions, or patent disclosures:

Do you have any discoveries, inventions, or patent disclosures to report for this period?

No

Please describe and include any notable dates

Do you plan to pursue a claim for personal or organizational intellectual property?

Changes in research objectives (if any):

Change in AFOSR Program Officer, if any:

Extensions granted or milestones slipped, if any:

AFOSR LRIR Number

LRIR Title

Reporting Period

Laboratory Task Manager

Program Officer

Research Objectives

## Technical Summary

### Funding Summary by Cost Category (by FY, \$K)

	Starting FY	FY+1	FY+2
Salary			
Equipment/Facilities			
Supplies			
Total			

## Report Document

### Report Document - Text Analysis

### Report Document - Text Analysis

## Appendix Documents

## 2. Thank You

### E-mail user

Feb 26, 2017 00:51:46 Success: Email Sent to: jgilles@mail.sdsu.edu